

This discussion paper is/has been under review for the journal Atmospheric Chemistry and Physics (ACP). Please refer to the corresponding final paper in ACP if available.

Long term in-situ observations of biomass burning aerosol at a high altitude station in Venezuela – sources, impacts and inter annual variability

T. Hamburger¹, M. Matisāns¹, P. Tunved¹, J. Ström¹, S. Calderon², P. Hoffmann², G. Hochschild³, J. Gross³, T. Schmeissner⁴, and R. Krejci^{1,5}

¹Department of Applied Environmental Science (ITM), Stockholm University, 106 91 Stockholm, Sweden

²Universidad de Los Andes, Merida 5101, Venezuela

³Karlsruhe Institute of Technology, Institute for Meteorology and Climate Research (ASF), 76344 Eggenstein-Leopoldshafen, Germany

⁴Leibniz Institute for Tropospheric Research (TROPOS), 04318 Leipzig, Germany

⁵Division of Atmospheric Sciences Department of Physics, University of Helsinki, 00014 Helsinki, Finland

ACPD
13, 13079–13117, 2013

Discussion Paper | Discussion Paper

Observations of biomass burning aerosol

T. Hamburger et al.

Title Page

Abstract

Introduction

Conclusions

References

Tables

Figures

◀

▶

◀

▶

Back

Close

Full Screen / Esc

Printer-friendly Version

Interactive Discussion



Received: 30 April 2013 – Accepted: 7 May 2013 – Published: 17 May 2013

Correspondence to: T. Hamburger (thomas.hamburger@itm.su.se)

Published by Copernicus Publications on behalf of the European Geosciences Union.

ACPD

13, 13079–13117, 2013

Observations of biomass burning aerosol

T. Hamburger et al.

Title Page

Abstract

Introduction

Conclusions

References

Tables

Figures



Back

Close

Full Screen / Esc

[Printer-friendly Version](#)

Interactive Discussion



Abstract

First long-term observations of South American biomass burning aerosol within the tropical lower free troposphere are presented. The observations were conducted between 2007 and 2009 at a high altitude station (4765 m a.s.l.) on the Pico Espejo, Venezuela. Sub-micron aerosol volume, number concentrations of primary particles and particle absorption were observed. Orographic lifting and shallow convection leads to a distinct diurnal cycle at the station. It enables measurements within the lower free troposphere during night time and observations of boundary layer air masses during day time and at their transitional regions. The seasonal cycle is defined by a wet rainy season and a dry biomass burning season. The particle load of biomass burning aerosol is dominated by fires in the Venezuelan savannah. Increases of aerosol concentrations could not be linked to long-range transport of biomass burning plumes from the Amazon basin or Africa due to effective wet scavenging of particles. Highest particle concentrations were observed within boundary layer air masses during the dry season. Ambient sub-micron aerosol volume reached $1.4 \pm 1.3 \mu\text{m}^3 \text{cm}^{-3}$, heated (300 °C) particle number concentrations $510 \pm 420 \text{ cm}^{-3}$ and the absorption coefficient $0.91 \pm 1.2 \text{ Mm}^{-1}$. The respective concentrations were lowest within the lower free troposphere during the wet season and averaged at $0.19 \pm 0.25 \mu\text{m}^3 \text{cm}^{-3}$, $150 \pm 94 \text{ cm}^{-3}$ and $0.15 \pm 0.26 \text{ Mm}^{-1}$. A decrease of particle concentrations during the dry seasons from 2007–2009 could be connected to a decrease in fire activity in the wider region of Venezuela using MODIS satellite observations. The variability of biomass burning is most likely linked to the El Niño-Southern Oscillation (ENSO). Low biomass burning activity in the Venezuelan savannah was observed to follow La Niña conditions, high biomass burning activity followed El Niño conditions.

Observations of biomass burning aerosol

T. Hamburger et al.

[Title Page](#)

[Abstract](#)

[Introduction](#)

[Conclusions](#)

[References](#)

[Tables](#)

[Figures](#)

◀

▶

◀

▶

[Back](#)

[Close](#)

[Full Screen / Esc](#)

[Printer-friendly Version](#)

[Interactive Discussion](#)



1 Introduction

Atmospheric aerosol particles directly scatter and absorb sunlight (Haywood and Boucher, 2000) or indirectly perturb the solar radiation by changing the formation and life cycle of clouds (Lohmann and Feichter, 2005). Thus, knowledge on their physical and chemical properties and temporal and spatial variability is of major importance when investigating the earth-climate system. Relative to greenhouse gases, particles in the atmosphere can be considered as a rather short-lived radiatively active species. Their properties feature a high variability in space and time. This makes the quantitative estimate of their climatic effects highly uncertain (Andreae et al., 2005). Recent and ongoing work helps to reduce these uncertainties (Myhre, 2009).

Within the present work we focus on observations of light absorbing aerosol particles within the tropical planetary boundary layer and lower free troposphere. Absorbing aerosols, as aerosol particles in general, reduce the incoming solar radiation on the surface and thus lead to a surface cooling. In addition, the absorbing particles heat the air at upper levels due to absorption of solar radiation. Hence, they alter the vertical temperature profile, latent heat fluxes, atmospheric stability and large-scale convection (Menon et al., 2002). Absorbing aerosol may also decrease low level cumulus cloud cover by heating the upper boundary layer which reduces the ambient relative humidity (Ackerman et al., 2000).

The main absorbing aerosol in the atmosphere is black carbon (BC). It's contribution to global warming may be substantial (Chameides and Bergin, 2002). Unlike greenhouse gases which absorb infra-red radiation, BC warms by absorbing sunlight. BC is the main absorbing component of soot next to several other absorbing condensed organic components (Andreae and Gelencsér, 2006; Ramanathan and Carmichael, 2008). Soot is produced through incomplete combustion of biomass, coal, and diesel fuel. The radiative and chemical properties of soot and its content of BC crucially depend on the source of the fuel (Chameides and Bergin, 2002) and the efficiency of the combustion process (Novakov et al., 2003). The resulting properties of the soot par-

Observations of biomass burning aerosol

T. Hamburger et al.

[Title Page](#)

[Abstract](#)

[Introduction](#)

[Conclusions](#)

[References](#)

[Tables](#)

[Figures](#)

◀

▶

◀

▶

[Back](#)

[Close](#)

[Full Screen / Esc](#)

[Printer-friendly Version](#)

[Interactive Discussion](#)



Observations of biomass burning aerosol

T. Hamburger et al.

[Title Page](#)

[Abstract](#)

[Introduction](#)

[Conclusions](#)

[References](#)

[Tables](#)

[Figures](#)

◀

▶

◀

▶

[Back](#)

[Close](#)

[Full Screen / Esc](#)

[Printer-friendly Version](#)

[Interactive Discussion](#)



ticles are defined by the mainly unknown shape (van Poppel et al., 2005). In addition to their radiative impacts, soot particles also play a large role in air quality and human health issues (Shindell et al., 2012).

One of the dominating sources of soot is biomass burning, i.e. open burning of forest, savannah and agricultural areas. Biomass burning produces ~40 % of the global BC emissions (Bond et al., 2004). Model simulations using in-situ observations of brown clouds which result from biomass burning in Asia showed that these clouds may contribute as much as the recent increase of anthropogenic greenhouse gases to regional lower atmospheric warming trends (Ramanathan et al., 2007). Large radiative impacts were observed above land in the biomass burning areas of Africa and South America and over the ocean downwind the biomass burning regions (Bellouin et al., 2005). Biomass burning in South America itself contributes 30 % to the global total biomass burning activities (Rissler et al., 2006) and 20–25 % to global BC emissions (Koch et al., 2007; Bond et al., 2004).

Next to biomass burning in the Amazon region, which is a major source of pollution in the tropical Southern Hemisphere (Streets et al., 2004; Edwards et al., 2006), biomass burning in the savannah region of northern South America contributes to a considerable amount to the pollution level in the tropical Northern Hemisphere (Hao and Liu, 1994). Most fires in the savannah region are of anthropogenic origin, e.g. to control weeds and pest, to prevent litter accumulation, or to accelerate nutrient cycling (Sanhueza et al., 1999). In-situ observations in the savannah region of the Venezuelan low lands proved a substantial contribution of biomass burning to the particle load at remote sites (Sanhueza et al., 1987; Morales et al., 1990). Biomass burning plumes originating from this area were observed at high altitudes during several airborne field campaigns (e.g. Andreae et al., 2001). However, to our best knowledge, there exist no long-term in-situ data of air masses effected by biomass burning in northern South America.

In this paper we provide the analysis of in-situ observations which were conducted at a high altitude station (4765 m a.s.l.) downwind the savannah plains of Venezuela. The observations were conducted between 2007–2009 and comprise two rainy seasons

and three dry seasons. Thus, we provide the first long-term in-situ observations of soot particles from biomass burning mixing into the lower free tropical troposphere above South America.

2 Methods

5 2.1 Measurement site

The Pico Espejo Atmospheric Research Station Alexander von Humboldt is located at 8° 31' N and 71° 3' W at an altitude of 4765 m a.s.l. (Calderón et al., 2008; Schmeissner et al., 2011) close to Venezuela's highest mountain, Pico Bolívar (4 981 m a.s.l.). The measurement station was rebuilt in 2001 by the Universidad de los Andes (ULA) in collaboration with the University of Karlsruhe and the Research Centre Karlsruhe (FZK), Germany, which in the meantime have merged into the Karlsruhe Institute of Technology (KIT). It can be reached by the Mérida Cable Car which was closed to public use in 2008. The city of Mérida is located approximately 10 km north-west of the Pico Espejo and is the largest populated area in the closer vicinity with a population reaching almost 200 000 inhabitants. The next densely populated urban areas and possible source regions of urban aerosol are the cities of San Cristóbal (~ 600 000), Venezuela, and Cúcuta (~ 1.1 mio), Colombia, both 150 km to the South-west and the metropolitan area of Maracaibo (~ 2.1 mio), Venezuela, 250 km to the North (Fig. 1). A vast tropical grassland plain (*Los Llanos*), which is mostly of agricultural use, extends to the South and South-east of the mountain range. This Venezuelan savannah is located between the Amazon forest in the South and the Caribbean Sea in the North. The climatological seasons in the region are defined by a rainy season from May to November and a dry season from December to April (Morales et al., 1990). Frequent biomass burning occurs in the end of the dry season mainly between March and May. The fires are located in the savannah region which reaches from the mountain ridge of the Andes in the West and follows the Orinoco river basin to the East (Rondón and Sanhueza,

Observations of biomass burning aerosol

T. Hamburger et al.

[Title Page](#)

[Abstract](#)

[Introduction](#)

[Conclusions](#)

[References](#)

[Tables](#)

[Figures](#)

◀

▶

◀

▶

[Back](#)

[Close](#)

[Full Screen / Esc](#)

[Printer-friendly Version](#)

[Interactive Discussion](#)



1990). The prevailing wind direction is governed by the northern hemispheric Trade winds; most of the time the wind blows from ENE (Sanhueza et al., 1987). Hence, the Venezuelan savannah serves as an important source region of biomass burning aerosol upwind the measurement site. Source regions of marine aerosol are rather distant, with the Pacific 800 km to the West, the Caribbean 400 km to the North and the Atlantic more than 1 000 km to the West.

2.2 Instrumentation

The aerosol instrumentation was provided by the Department of Applied Environmental Science (ITM), Stockholm University (Schmeissner et al., 2011). The aerosol was sampled through a 6 m long vertical inlet which was heated to 15 °C. The air reached the aerosol instrumentation at a relative humidity between 10–20 %.

Ambient aerosol number size distributions were observed with a custom-built Differential Mobility Particle Sizer (DMPS) system. The ambient DMPS was set to a size spectrum for particle diameters between 10 nm and 500 nm. The DMPS system was operated with one Condensation Particle Counter (CPC) model 3010, TSI Inc. A second CPC was used in combination with a Thermo denuder which heated the sampled aerosol to 300 °C. The volatile and semi-volatile aerosol compounds were evaporated before the sampled probe reached the second CPC. The thermo denuder was installed behind the Differential Mobility Analyser (DMA) of the DMPS. Hence, the upper cut-off diameter of the residual particles was limited by the diameter range of the DMPS.

The residual particles consist mainly of primary aerosol. Those primary particles most commonly consist of dust, sea spray and soot. BC from combustion processes however is the most abundant primary particle species in the observed size range from 10–500 nm. Previous observations showed that particle size distributions resulting from vegetation fires have a mean geometric diameter of 120–230 nm (Jahñall et al., 2010). Particles on the larger end of the diameter range are associated with rather aged biomass burning plumes (days) and smaller diameters with fresh plumes (hours). The size range of biomass burning particles falls into the size range of the

Observations of biomass burning aerosol

T. Hamburger et al.

Title Page

Abstract

Introduction

Conclusions

References

100

Figures

1

1

Back

Clos

三

/ Esc

Full Screen / Esc

卷之三

Interactive Discussion



observations presented here. However, the appearance of larger primary particles in the super-micrometer diameter range like sea salt and dust can not be completely neglected. Although they are rather unlikely to be observed at the high altitude station due to its remote location.

5 The aerosol absorption coefficient b_{abs} was measured by a filter based technique using a custom-build Particle Soot Absorption Photometer (PSAP). The PSAP measures the light extinction of aerosol particles at a wavelength of $\lambda = 525 \text{ nm}$. The particle filters were mounted in a revolver like system allowing for automatic filter change. A transmission value of $\text{Tr} = 0.5$ was set as threshold for each filter change.

10 An automatic weather station detected standard meteorological parameters including pressure, temperature, relative humidity, wind speed and wind direction, and direct and diffuse radiation. In addition two webcams were installed at the research station facing the northern and southern slopes of the Pico Espejo. The webcams saved pictures in 15 min intervals. A Photometric Ozone Analyser completed the instrumentation 15 setup. Results of the Ozone measurements can be found in Calderón et al. (2008).

The observations were carried out from March 2007 until May 2009. A routine check was performed every 5th day on average. All concentrations are given at ambient conditions. To convert from ambient to standard temperature and pressure ($T_{\text{stp}} = 273.15 \text{ K}$, $p_{\text{stp}} = 1013.25 \text{ hPa}$) use $\text{stp} = 1.77 (\pm 0.01) \text{ amb}$.

20 2.3 Data analysis

The data inversion method of DMPS measurements is described in Schmeissner et al. (2011). They note that 13 % of the DMPS observations had to be excluded due to erroneous data.

25 The PSAP measurements were corrected following the correction schemes by Bond et al. (1999), Virkkula et al. (2005), and Virkkula (2010). The ambient DMPS size distribution was used to estimate the scattering coefficient for the scattering correction. The refractive index of Ammonium sulphate (1.42 ± 0.006) was applied. However, the upper cut off diameter of the DMPS lies well below the upper cut off diameter of the aerosol

Observations of biomass burning aerosol

T. Hamburger et al.

[Title Page](#)

[Abstract](#)

[Introduction](#)

[Conclusions](#)

[References](#)

[Tables](#)

[Figures](#)



[Back](#)

[Close](#)

[Full Screen / Esc](#)

[Printer-friendly Version](#)

[Interactive Discussion](#)



inlet. This may cause an underestimation of the scattering coefficient and therefore may result in an overestimation of the absorption coefficient ($\sim 10\%$). A distinctive decrease in the changing rate of the transmission was observed for $Tr < 0.7$ during the processing of the raw data. The reduced changing rate resulted in an underestimation of the calculated absorption coefficient at $Tr < 0.7$. Thus, the threshold value of the transmission was set to $Tr = 0.7$ to avoid bias induced by strongly polluted filters. In addition, 30 % (~ 155 out of 510 days) of the PSAP data had to be excluded due to malfunction of the filter change procedure or malfunction of the recording of the sampled air flow through the PSAP instrument.

We resign to convert b_{abs} to the mass concentration of BC, though BC dominates the absorption of light on the filter. The conversion of b_{abs} to BC mass relies on the mass absorption coefficient (MAC) which undergoes large variabilities depending on the optical properties of the sampled soot (Mertes et al., 2004; Bond and Bergstrom, 2006; Schwarz et al., 2008; Naoe et al., 2009; Yang et al., 2009). However, the lack of chemical information present does not allow for an accurate definition of MAC.

Break-up of cloud droplets on the aerosol inlet and subsequent sampling of the droplet particles can only be strong bias to the observations. Therefore, in-cloud data had to be removed. In-cloud sequences were determined using the webcam images and a cloud detection algorithm. Due to practical limitations the cloud detection algorithm was applied to daytime data, only. Hence, the relative humidity had to serve as threshold value for night-time data. The assigned in cloud sequences had a median relative humidity of $RH \sim 97\%$. When no suitable webcam image was available all observations with $RH > 95\%$ were marked as in-cloud sequences and the respective data were excluded for the subsequent analysis.

Applying the correction and the elimination of errors of the DMPS and PSAP raw data in combination with the exclusion of cloud data a total of 20 % of the original PSAP raw data could be used for the following analysis. Nevertheless, the PSAP data covers all rainy and dry seasons which were observed.

Observations of biomass burning aerosol

T. Hamburger et al.

[Title Page](#)

[Abstract](#)

[Introduction](#)

[Conclusions](#)

[References](#)

[Tables](#)

[Figures](#)

◀

▶

◀

▶

[Back](#)

[Close](#)

[Full Screen / Esc](#)

[Printer-friendly Version](#)

[Interactive Discussion](#)



Observations of biomass burning aerosol

T. Hamburger et al.

The observations were divided into two distinct air masses that possibly reach the high altitude station: air masses of the lower free troposphere (LFT) and air masses from the boundary layer (BL). The separation was defined by using the typical diurnal cycle which could be observed at the site. It is described in Sect. 3.4. Measurements were assigned to the BL if they were observed between 10:00 and 23:00 local time and if the relative humidity (RH) did not reach below 65 %. Night time data and data at $RH < 65\%$ were considered as observations within the LFT.

2.4 Air mass transport analysis and satellite observations

We used the well known HYSPLIT trajectory model (Draxler, 1999) to analyse the history of the air masses that reach the high altitude station. The calculations were based on the meteorological fields from the National Centers for Environmental Prediction (NCEP). The meteorological fields had a spatial resolution of $1^\circ \times 1^\circ$ and a temporal resolution of 3 h.

Two altitude ranges were set as starting positions for the HYSPLIT back trajectories according to the separation of the air masses into BL and LFT. One starting point was set to the given altitude of the research station (4765 m a.s.l.) which lies above the altitude of the model mixing layer. Hence, the back trajectories starting from the top of the mountain represent the air mass transport in the lower free troposphere. The second starting point is variable and was set to half the model mixing layer depth above the model surface altitude at the given date and time. This assures that the second starting point lies within the boundary layer. The back trajectories starting from the second lower position account for air masses originating from the planetary boundary layer. The air masses reach the station due to nearby shallow convection or small scale orographic lifting. None of these regional effects are represented by the global meteorological fields which served as input data.

The trajectories were calculated backwards for 240 h starting in 3 h intervals. They contain information on meteorological parameters along the transport pathway like relative humidity or surface precipitation. We included satellite observations into the tra-

13088

 CC BY

Observations of biomass burning aerosol

T. Hamburger et al.

[Title Page](#)

[Abstract](#)

[Introduction](#)

[Conclusions](#)

[References](#)

[Tables](#)

[Figures](#)

◀

▶

◀

▶

[Back](#)

[Close](#)

[Full Screen / Esc](#)

[Printer-friendly Version](#)

[Interactive Discussion](#)



jectory analysis to extend the information of the air mass history by biomass burning – one of the main aerosol sources in the tropics (Bond et al., 2013).

We used the Global Monthly Fire Location Product (MCD14ML, Giglio et al., 2003, 2006; Giglio, 2010) and Burned Area Product (MCD45A1, Roy et al., 2005, 2008) which are retrieved from the Moderate Resolution Imaging Spectroradiometer (MODIS) observations on the Terra and Aqua satellites. The Global Monthly Fire Location Product was used in combination with the computed back trajectories to retrieve the respective information on air mass history. Precipitation data given by the HYSPLIT model was used to reduce possible impact of precipitation on the particle load along the transport pathway. It is based on the NCEP data. Fires along the transport pathway were only considered if no precipitation occurred between the fire event and the observation at the measurement site and if the trajectory was located within the boundary layer when passing over a biomass burning area. The Global Monthly Fire Location Product was extrapolated to a $0.1^\circ \times 0.1^\circ$ grid for the combination with the trajectories. In addition, fires that were detected up to three days prior to the trajectory overpass were considered. The result is the number of fire events since the last precipitation event (Sect. 4). Fire pixels were considered if their estimated detection confidence was nominal or high, i.e. greater than 30 % (see Giglio, 2010).

The MODIS Burned Area Product was used to estimate the burned area per month in the Venezuelan savannah for the period between 2000–2013. We considered a region between $6\text{--}11^\circ\text{N}$ and $62\text{--}72.5^\circ\text{W}$ ($\sim 640 \times 10^3 \text{ km}^2$) which covers most of the savannah upwind the observation site. The fire pixels have a horizontal resolution of 500 m. Multiple counts of the same fire pixel per month were omitted. We use the burned area to discuss the three observed biomass burning seasons within a wider climatological context (Sect. 5.2).

Observations from the Cloud-Aerosol Lidar and Infrared Pathfinder Satellite Observation (CALIPSO) satellite (Winker et al., 2009) were used to investigate the average expansion of lifted aerosol layers downwind the observation site. We used the Lidar Level 2 5 km Aerosol Layer Product. We were interested in aerosol layers at a similar

altitude like the top of the mountain range which frequently compares to the top of the boundary layer. The top layer altitude and the surface elevation from GTOPO30 digital elevation map (DEM), both provided by the Aerosol Layer Product, were used to calculate the altitude above the surface of the upper most aerosol layer. In addition, we applied the Feature Classification Flags (Mielonen et al., 2009; Omar et al., 2009) to estimate the most frequent aerosol type of the upper most aerosol layer at the respective location. Data for the months February–April, i.e. the months of the main biomass burning period in Venezuela (Morales et al., 1990), were averaged over the years of the in-situ observations 2007–2009 (Sect. 5.1).

10 3 Results of in-situ observations

3.1 Meteorological conditions

The meteorological conditions at the Pico Espejo and their seasonal variations are controlled by the North–South shift of the Intertropical Convergence Zone (ITCZ). The ITCZ is associated with the ascending branch of the Hadley Cell. It is characterised by deep convection and subsequent strong precipitation events. The ITCZ is located south of the Pico Espejo during northern hemispheric winter. Decreased convective activity and enhanced subsidence of air masses lead to rather dry conditions within the lower troposphere. The trade winds transport air masses from ENE to Venezuela. The influence of the ITCZ gets more prominent during the northern hemispheric summer when it migrates towards the North. It forces deep convection and precipitation in the region and leads to a change of the air mass origin as trade winds from ESE dominate the air mass transport. The effect of the migrating ITCZ and the subsequent change in ambient humidity can be clearly seen in the seasonal variation of the relative humidity RH in the LFT (Figs. 2 and 3). Typical for tropical regions, the seasonal cycle of the meteorological conditions at Pico Espejo can be divided into a dry and wet season. The

Observations of biomass burning aerosol

T. Hamburger et al.

[Title Page](#)

[Abstract](#)

[Introduction](#)

[Conclusions](#)

[References](#)

[Tables](#)

[Figures](#)

◀

▶

◀

▶

[Back](#)

[Close](#)

[Full Screen / Esc](#)

[Printer-friendly Version](#)

[Interactive Discussion](#)



dry season peaks from January till March and the wet season reaches its maximum between July and September.

The orography causes a pronounced diurnal cycle besides the seasonal cycle. Due to the high altitude of the research station measurements are mostly performed within the lower free troposphere during the night. However, during daytime surface heating and subsequent convection lead to an orographically driven upslope flow as air masses originating from the planetary boundary layer are lifted upwards and reach the station (Fig. 4).

3.2 Seasonal cycle

- 10 Table 1 summarises the mean values of each season observed within the BL and the LFT. Whilst the relative humidity and ambient temperature remain constant throughout the seasons for BL air masses ($\text{RH} = 82\text{--}86\%$, $t \sim 2^\circ\text{C}$), they differ within the LFT. RH shows a high variability in the LFT for both, dry and wet season with a standard deviation between 25–27 % (see also time series in Fig. 2). However, RH increases from 45 % to 67 % from the dry to the wet season. The temperature remains constant at $t \sim 0^\circ\text{C}$.
- 15

- The dry biomass burning season has a large impact on all observed aerosol parameters within the BL and LFT with maxima values within the BL, as expected. The aerosol volume V reaches an average of $0.49 \mu\text{m}^3 \text{cm}^{-3}$ in the wet and $1.4 \mu\text{m}^3 \text{cm}^{-3}$ during the dry season. The absorption coefficient b_{abs} increases from 0.32Mm^{-1} to 0.91Mm^{-1} (factor 2.8) from the wet to the dry season. However, both parameter show a standard deviation of $\sim 100\%$. Recent studies showed an increase of b_{abs} from the wet to the dry season from 0.5Mm^{-1} to 2.8Mm^{-1} (factor 5.6) in the Amazon rain forest at 110 m a.s.l. (Rizzo et al., 2012) which is twice the increase of b_{abs} compared to our observations of biomass burning in the savannah. The trajectory analysis shows the highest average number of fire events since the last precipitation event of 3 for the
- 20
- 25

[Title Page](#)[Abstract](#)[Introduction](#)[Conclusions](#)[References](#)[Tables](#)[Figures](#)[|◀](#)[▶|](#)[Back](#)[Close](#)[Full Screen / Esc](#)[Printer-friendly Version](#)[Interactive Discussion](#)

Observations of biomass burning aerosol

T. Hamburger et al.

[Title Page](#)

[Abstract](#)

[Introduction](#)

[Conclusions](#)

[References](#)

[Tables](#)

[Figures](#)

◀

▶

[Back](#)

[Close](#)

[Full Screen / Esc](#)

[Printer-friendly Version](#)

[Interactive Discussion](#)



dry BL which is consistent to the increased particles load during the biomass burning season.

The average values within the wet LFT can be considered as mean background values which are rather stable throughout the year. The aerosol volume V reaches an average of $0.19 \mu\text{m}^3 \text{cm}^{-3}$ and the average absorption coefficient b_{abs} is 0.15Mm^{-1} .

3.3 Inter annual variability

Figures 2 and 3 show the respective time series of relative humidity (RH), ambient aerosol volume concentration for particles smaller 500 nm (V), heated aerosol number concentration ($N_{300^\circ\text{C}}$), and the absorption coefficient (b_{abs}) for the LFT and BL. Each time series shows the single data (15 min average) and the adjacent average over one month as well as its standard deviation.

The average RH varies in the LFT between 30–80 % comparing dry and wet season and features a high variability throughout the observation period. The wet seasons of 2007 and 2008 show no significant difference in the maximum relative humidity. However, the dry season of 2008 ($\text{RH}_{\min} \sim 30\%$) features drier air masses on average than the dry season of 2009 ($\text{RH}_{\min} \sim 40\%$). Both dry seasons also show different months of lowest RH with the beginning of February in 2008 and the end of December 2008 for the dry season of 2009. The minimum RH in 2007 can not be assigned. RH was 45 % at the beginning of the observations in March 2007. The RH in the BL features a relatively small inter annual variability. Its average lies between 80–90 %.

The enhancement of particulate matter during the dry season within the BL is also reflected in the LFT. The air masses mix due to (dry) convection and orographic lifting induced by the mountain range. Thus, primary particles such as soot are mixed into the LFT. However, the total concentration is diluted by the rather clean and dry free tropospheric air. The particle volume concentrations in the BL (Fig. 3) reach their respective maxima in mid March 2007, end of March 2008 and mid of April 2009. The dry season maxima decrease continuously from 2007 to 2009 ($2.9/2.6/2.1 \mu\text{m}^3 \text{cm}^{-3}$). A similar trend can be observed for $N_{300^\circ\text{C}}$ ($1300/720/470 \text{cm}^{-3}$). b_{abs} also shows its

maximum in the dry season of 2007 (3.8 Mm^{-1}). However, b_{abs} features an increase from 2008 to 2009 from 2.0 Mm^{-1} to 2.6 Mm^{-1} . I.e., an overall decrease of biomass burning aerosol was observed from 2007–2009.

The inter annual variability will be further discussed using satellite observations in Sect. 5.2.

3.4 Diurnal cycle

The mixing of the two air masses, BL and LFT, can be observed by examining the diurnal cycles in Fig. 4. The data were split into wet (blue) and dry (red) season. The relative humidity showed a clear diurnal cycle particularly during the dry season. During

the night, which may be considered as free tropospheric air, the minimum of the hourly average dropped to $\text{RH} = 55\%$ at 06:00 LT (local time). The average relative humidity increased during daytime to a maximum of $\text{RH} = 81\%$ at 16:00 LT when boundary layer air masses were lifted to the station.

The variations between the average minima and maxima during the wet season were respectively: $V = 0.15\text{--}0.78 \mu\text{m}^3 \text{cm}^{-3}$, $N_{300^\circ\text{C}} = 120\text{--}300 \text{cm}^{-3}$, $b_{\text{abs}} = 0.09\text{--}0.52 \text{Mm}^{-1}$. Twice as high concentrations were observed for the average minima and maxima during the dry season: $V = 0.30\text{--}1.84 \mu\text{m}^3 \text{cm}^{-3}$, $N_{300^\circ\text{C}} = 190\text{--}620 \text{cm}^{-3}$, $b_{\text{abs}} = 0.16\text{--}1.30 \text{Mm}^{-1}$.

The minima could be observed during night time till the early morning hours. The mixing of boundary layer air into free tropospheric air begins between 09:00–10:00 LT. Interestingly, the observed aerosol concentrations reach their maxima during the wet season between 16:00–17:00 LT and during the dry season between 14:00–16:00 LT. However, due to the location close to the equator there is only little time shift in sunrise (less than one hour) within the year with earlier sunrise during the wet season. This would even trigger rather earlier than late convection during the wet season. Increased cloud cover and latent heat production delays the rise of the boundary layer. Although the sunshine intensity is slightly stronger during the wet season a considerable amount

Observations of biomass burning aerosol

T. Hamburger et al.

[Title Page](#)

[Abstract](#)

[Introduction](#)

[Conclusions](#)

[References](#)

[Tables](#)

[Figures](#)

◀

▶

[Back](#)

[Close](#)

[Full Screen / Esc](#)

[Printer-friendly Version](#)

[Interactive Discussion](#)



of solar radiation is scattered by clouds or required to evaporate water in the morning hours from the moist surface during the wet season. This energy is already available during the morning hours in the dry season to produce sensible heat on the dry surface and to drive convection on the mountain slope. Thus, the boundary layer reaches the 5 mountain station about two hours earlier during the dry season than during the wet season.

4 Identification of source regions

A possible source region of South American biomass burning plumes reaching the research station are the savannah regions of Venezuela (Sanhueza et al., 1987) as explained before. In addition, biomass burning events further to the South in the Amazon 10 region which contributes with about 30 % to the global total biomass burning activities (Rissler et al., 2006) may serve as possible sources. Long-range transport of biomass burning aerosol and dust from northern and tropical Africa to South America via the Atlantic was observed by foregoing studies, too (Edwards et al., 2006; Ansmann et al., 15 2009; Adams et al., 2012; Rizzo et al., 2012).

We used HYSPLIT trajectories in combination with the MODIS Global Monthly Fire Location Product to detect possible source regions during the dry and wet season. Figure 5a and b show fire events within the last 10 days that possibly effected the air masses reaching the Pico Espejo. The analysis is divided into two subsets; one 20 considering precipitation between the source and the observation site (Fig. 5a) and one not considering the precipitation during the air mass transport (Fig. 5b). In both cases the main source region is the Venezuelan savannah during the dry season. A non-negligible amount of fire events are located in the Amazon basin. However, with the observation site located north of the equator and the Amazon basin in the Southern 25 Hemisphere, the biomass burning season in the Amazon basin coincides with the wet season in Venezuela. Hence, particulate matter from Amazonian biomass burning is very likely to be scavenged by precipitation during the transport towards Venezuela.

Observations of biomass burning aerosol

T. Hamburger et al.

[Title Page](#)

[Abstract](#)

[Introduction](#)

[Conclusions](#)

[References](#)

[Tables](#)

[Figures](#)

◀

▶

[Back](#)

[Close](#)

[Full Screen / Esc](#)

[Printer-friendly Version](#)

[Interactive Discussion](#)



Observations of biomass burning aerosol

T. Hamburger et al.

Title Page	
Abstract	Introduction
Conclusions	References
Tables	Figures
◀	▶
◀	▶
Back	Close
Full Screen / Esc	
Printer-friendly Version	
Interactive Discussion	



Considering the trajectory analysis long-range transport from West Africa seems possible. Additional analysis not shown here using the FLEXPART dispersion model (Stohl et al., 2005) indicates possible impact from African biomass burning, too. However, no signal in the particle properties could be significantly connected to those events. The particle observations are dominated by the regional biomass burning and thus may mask the signal of long-range transport during the dry season. During the rainy season most particulate matter is removed by wet scavenging leaving long-lived trace gases like CO in the atmosphere as possible tracers of biomass burning which were not observed at the station.

We compared relative humidity, the aerosol volume concentration, the number concentration of heated particles, and the absorption coefficient to the number of fire events along the transport pathway since the last precipitation event. The concentrations are binned into intervals of 5 fire events, each. Averages were calculated for each bin if the number of observations (each observation being a 15 min average) exceeded 20. Most back trajectories associated with biomass burning events were started within the model boundary layer. The relative humidity indicates this feature with a constant relative humidity greater than 80 % for 5 and more biomass burning events. Less biomass burning events (0–5) indicate drier air masses which can be partly associated with the free troposphere. The aerosol volume concentration V shows an increase from $0.5 \mu\text{m}^3 \text{cm}^{-3}$ at 0–5 fire events to $2.7 \mu\text{m}^3 \text{cm}^{-3}$ at 55–60 fire events. The average of the number concentration of heated particles $N_{300^\circ\text{C}}$ increases from 270 cm^{-3} at 0–5 fire events to a maximum of 1200 cm^{-3} at 50–55 fire events. Only few bins of fire events could be connected to b_{abs} measurements. However, an increase of the average b_{abs} with increasing number of fire events can be observed, too, from 0.4 Mm^{-1} at 0–5 fire events to a maximum of 1.8 Mm^{-1} at 10–15 fire events.

The high variability of the trajectory analysis, caused amongst others by the uncertainty of the trajectories, does not allow for a significant correlation throughout the whole number spectrum of fire events. Nevertheless, the trajectory analysis shows that

the main source of absorbing primary particulate matter at the Pico Espejo is biomass burning from the nearby Venezuelan savannah region.

5 Analysis of satellite observations

In the following section we will identify the regions that are possibly affected by the uplifted biomass burning plumes using CALIPSO satellite observations. In addition we examine the biomass burning intensity in the wider region of Venezuela of the last 12 yr (end of 2000 until beginning of 2013) with the help of MODIS satellite products to put the presented in-situ observations into a climatological context.

5.1 Transport of smoke plumes downwind the source region

The soot particles emitted by the biomass burning fires can directly affect the radiative transfer above a region by absorbing light and thus heating the ambient air which possibly leads to a reduction of the cloud cover or can change regional cloud properties by providing additional cloud condensation nuclei (Ten Hoeve et al., 2012). The resulting effect depends on the radiative properties of the respective biomass burning plume. But, not only the individual properties of the biomass burning plume are important. Depending on its location and underlying surface, e.g. ocean or land, their overall regional radiative effects can differ in sign. Sakaeda et al. (2011) found that biomass burning plumes above the ocean frequently appear as elevated layers above underlying cloud layers, thus having a negative top of the atmosphere radiative effect, whereas the increase in cloud albedo above land has a positive top of the atmosphere radiative effect. In addition, elevated biomass burning layers might have an potential of further lifting and increasing persistence due to their ability of heating the ambient air by absorbing the solar radiation (Boers et al., 2010).

We use the CALIPSO Level 2 5 km Aerosol Layer product to estimate the region which can be affected by biomass burning plumes downwind Venezuela. The satellite

[Title Page](#)

[Abstract](#)

[Introduction](#)

[Conclusions](#)

[References](#)

[Tables](#)

[Figures](#)

◀

▶

◀

▶

[Back](#)

[Close](#)

[Full Screen / Esc](#)

[Printer-friendly Version](#)

[Interactive Discussion](#)



data was averaged for the months from February to April and the years 2007 to 2009. Figure 7a shows the altitude above the surface of the upper most aerosol layer. Maximum altitudes reaching more than 7 km can be observed above the Amazon region where the ITCZ is located at that time. The altitude is generally lower in the northern hemispheric South America during the dry season. The altitude above surface increases from the Venezuelan savannah plains towards the mountain range of the Andes from 2–3 km to 4–5 km. Downwind, i.e. WSW of the Andes, the uplifted aerosol layers maintain an altitude between 3–5 km above the surface of the Pacific ocean. The transport of the elevated aerosol layers with the trade winds can be observed with the satellite data for more than 1500 km almost reaching the Galápagos Islands.

The transport pathway is supported by 10 day forward trajectory calculations which are indicated by dashed clouds in Fig. 7a and b. The trajectories were started from the top of the model boundary layer at the location of the Pico Espejo to simulate the possible transport of the residual layers. The trajectory cloud represents the average region that can be reached between February and May by the biomass burning layers. It extends dominantly towards the WSW of the Pico Espejo as expected by the prevailing wind conditions.

The Aerosol Feature Classification product shows that the elevated aerosol layer downwind the northern hemispheric part of South America are mostly classified as “Smoke” (Fig. 7b). Those “Smoke” layers originate from biomass burning fires and contain to a great extend light absorbing soot.

5.2 12 yr of satellite observations – the in-situ measurements in a climatological context

The inter annual variability discussed in Sect. 3.3 shows a decrease in concentrations of primary absorbing aerosol particles from the dry season in 2007 to the dry season in 2009. This decrease in aerosol concentrations suggests an decrease in biomass burning activity in the main source region of the Venezuelan savannah plains. Figure 8 shows the burned area per month for the years 2000 to 2013. The area of interest

[Title Page](#)[Abstract](#)[Introduction](#)[Conclusions](#)[References](#)[Tables](#)[Figures](#)[|◀](#)[▶|](#)[◀](#)[▶](#)[Back](#)[Close](#)[Full Screen / Esc](#)[Printer-friendly Version](#)[Interactive Discussion](#)

spans a rectangle which comprises the region of the Venezuelan savannah. The maximum burned area per month decreases from the dry season 2007 to the dry season 2009 from 9 300 km² to 720 km². This decline of biomass burning area is consistent with the observed particle concentrations and explains most of the decrease.

Several reasons can lead to a change in biomass burning activity – most prominent the prevailing meteorological conditions. But also legal regulations due to environmental pressures and weakening demand for new agricultural land are causes to reduce regional biomass burning (Streets et al., 2004). E.g., Koren et al. (2007) found a reversal trend from formerly increasing biomass burning intensity in the Amazon Basin to a sharp decrease in 2006. They speculated that the decrease might result from a tri-national policy shift which was implemented in 2006 in the Amazon area. However, the authors mention that this abrupt decrease of fires may have also been the effect of a positive precipitation anomaly in the rainy season of the same year. Further, Torres et al. (2010) reported a huge increase of biomass burning activity in 2007 followed by a decline of fires in 2008 and 2009. Although the study comprises whole South America with a focus on the Amazon Basin the results match with our observations. Torres et al. (2010) suggest, that the strong decline in 2008 might be influenced by non-meteorological factors.

Since 2008, the Venezuelan State changed legal regulations related to forest fires (Ley de Bosques y Gestión Forestal, 2008). Modifications on the legal definition of fire protected areas as well as the creation of several types of fire-fighter leagues, including the forest ranger brigade and the communal brigades, could explain the decline of biomass burning. Those brigades are intended to help with environmental education, preventive surveillance, report of negative activities against the forest heritage and also with the supervision of all institutions related to the forest fire prevention and mitigation across the country. However, the regulations may only have an impact from the 2009 biomass burning season on. So far, the time series of the burned area per month does not show a continuous increase/decrease within the years 2000 to 2013 which might serve as an indication for a successful implementation of legal regulations.

Observations of biomass burning aerosol

T. Hamburger et al.

[Title Page](#)

[Abstract](#)

[Introduction](#)

[Conclusions](#)

[References](#)

[Tables](#)

[Figures](#)

◀

▶

◀

▶

[Back](#)

[Close](#)

[Full Screen / Esc](#)

[Printer-friendly Version](#)

[Interactive Discussion](#)



Observations of biomass burning aerosol

T. Hamburger et al.

[Title Page](#)

[Abstract](#)

[Introduction](#)

[Conclusions](#)

[References](#)

[Tables](#)

[Figures](#)

◀

▶

◀

▶

[Back](#)

[Close](#)

[Full Screen / Esc](#)

[Printer-friendly Version](#)

[Interactive Discussion](#)



Observations of biomass burning aerosol

T. Hamburger et al.

[Title Page](#)[Abstract](#)[Introduction](#)[Conclusions](#)[References](#)[Tables](#)[Figures](#)[|◀](#)[▶|](#)[◀](#)[▶|](#)[Back](#)[Close](#)[Full Screen / Esc](#)[Printer-friendly Version](#)[Interactive Discussion](#)

tions. This indicates that a lack of burning fuel and less demand on agricultural biomass burning can result in less burned area. On the other hand, all intense biomass burning seasons follow years featuring cold and wet La Niña conditions, when less biomass burning but more intense regrowth of grass and scrubs was possible. I.e. more burning fuel was available in the following years.

The overall trend of the years 2000 to 2012 and especially the link between the intense biomass burning season in 2007 with El Niño and the weak biomass burning seasons in 2008 and 2009 with La Niña indicate that the observed decrease of observed fire events and thus particle concentrations are dominated by ENSO related meteorological conditions and might mask local legal regulations.

6 Summary and conclusion

We presented the first long-term in-situ observations of biomass burning aerosol in the tropical lower free troposphere (LFT). The special location of the observation site at the Pico Espejo at an altitude of 4765 m a.s.l. allows for observations of free tropospheric air masses as well as boundary layer (BL) air masses. BL air masses reach the station during day time through orographic lifting and shallow convection. The Pico Espejo is located downwind the Venezuelan savannah where frequent biomass burning occurs during the end of the dry season between December and April. The Venezuelan savannah was found to be the main source region of biomass burning aerosol during the dry season. Fires in the Amazon basin, one of the major sources of southern hemispheric biomass burning emissions (Streets et al., 2004; Edwards et al., 2006), coincide with the wet season of the Northern Hemisphere. Hence, wet scavenging of particles during the transport of air masses from the Amazon basin towards the northern part of South America significantly reduced the aerosol concentrations. No evidence of long-range transport of biomass burning emissions in the LFT or BL could be found in the observed particle properties. However, long-lived trace species like CO were not observed.

Particle concentrations in the LFT were found to be rather low and stable. During the wet season the ambient sub-micron aerosol volume V averaged at $0.19 \pm 0.25 \mu\text{m}^3 \text{cm}^{-3}$, heated particle number concentrations at $N_{300\text{-}\text{C}}$ at $150 \pm 94 \text{ cm}^{-3}$ and the absorption coefficient b_{abs} at $0.15 \pm 0.26 \text{ Mm}^{-1}$. Maximum particle concentrations were found during the dry biomass burning season in BL air masses. They reached $V = 1.4 \pm 1.3 \mu\text{m}^3 \text{cm}^{-3}$, $N_{300\text{-}\text{C}} = 510 \pm 420 \text{ cm}^{-3}$ and $b_{\text{abs}} = 0.91 \pm 1.2 \text{ Mm}^{-1}$, respectively. The signal of the dry biomass burning season in the LFT is rather low compared to the BL although the seasonal variation of particle concentrations can be seen in the LFT. This indicates that on large scale the particle removal processes like wet scavenging in clouds work very effectively and limit the vertical transport of particles into the free troposphere.

CALIPSO satellite observations showed that layers of biomass burning aerosol were lifted on the upwind side of the northern end of the Andes. Those elevated “smoke” layers were transported downwind the Andes westward towards the Pacific ocean at an altitude of approximately 3–5 km. The biomass burning extended on average towards the Galápagos Islands and may perturb the solar radiation and atmospheric stability on a larger scale (Bellouin et al., 2005).

The observations at the Pico Espejo covered three dry seasons from 2007–2009. A distinct decrease of dry season particle concentrations was observed within this period. The analysis of fire activity in the wider region of Venezuela using MODIS satellite observations showed that the decrease of particle concentrations can be associated with a decrease in biomass burning activity. 12 yr of MODIS data indicated that the inter annual variability in biomass burning activity in this region can be linked to varying meteorological conditions induced by the El Niño-Southern Oscillation (ENSO). Low biomass burning activity in the Venezuelan savannah tended to follow La Niña conditions, high biomass burning activity followed El Niño conditions. In addition, legal regulations concerning biomass burning were passed by the Venezuelan government in 2006 and 2008. So far, the results of the legal regulations might be masked by the meteorological conditions. However, on a long-term base the benefits of the legal

Observations of biomass burning aerosol

T. Hamburger et al.

[Title Page](#)

[Abstract](#)

[Introduction](#)

[Conclusions](#)

[References](#)

[Tables](#)

[Figures](#)

◀

▶

◀

▶

[Back](#)

[Close](#)

[Full Screen / Esc](#)

[Printer-friendly Version](#)

[Interactive Discussion](#)



regulations and their impacts on the regional climate might be visible. Thus, future continuous observations, both, in-situ and remote sensing, are beneficial to examine the impact of legal regulations whilst considering inter annual variations of the meteorological conditions.

- 5 *Acknowledgements.* We thank the members of the CALIPSO and MODIS projects for giving us access to data products through their web ordering systems. The CALIPSO data were obtained from the NASA Langley Atmospheric Science Data Center (ASDC) (<http://www-calipso.larc.nasa.gov>). The MODIS data were obtained through the online Data Pool at the NASA Land Processes Distributed Active Archive Center (LP DAAC), USGS/Earth Resources Observation and
- 10 Science (EROS) Center, Sioux Falls, South Dakota (https://lpdaac.usgs.gov/get_data). Information on vegetation cover was retrieved from the NASA Global Land Data Assimilation System (GLDAS) (<http://ldas.gsfc.nasa.gov/gldas>). Changes to the Oceanic Niño Index (ONI) were provided by the National Oceanic and Atmospheric Administration (NOAA) National Weather Service Climate Prediction Center (http://www.cpc.ncep.noaa.gov/products/analysis_monitoring/ensostuff/ensoyears.shtml).
- 15 This work has been funded by the Swedish Research Council (VR, projects # 2004–4135 (OFTA) and # 2009–3007 (AVIAC)), the Swedish International Development Cooperation Agency (SIDA) and the Bolin Centre for Climate Research.

References

- 20 Ackerman, A. S., Toon, O. B., Stevens, D. E., Heymsfield, A. J., Ramanathan, V., and Welton, E. J.: Reduction of tropical cloudiness by soot, *Science*, 288, 1042–1047, doi:[10.1126/science.288.5468.1042](https://doi.org/10.1126/science.288.5468.1042), 2000. 13082
- Adams, A. M., Prospero, J. M., and Zhang, C.: CALIPSO derived three-dimensional structure of aerosol over the Atlantic and adjacent continents, *J. Climate*, 25, 6862–6879, doi:[10.1175/JCLI-D-11-00672.1](https://doi.org/10.1175/JCLI-D-11-00672.1), 2012. 13094
- 25 Andreae, M. O. and Gelencsér, A.: Black carbon or brown carbon? The nature of light-absorbing carbonaceous aerosols, *Atmos. Chem. Phys.*, 6, 3131–3148, doi:[10.5194/acp-6-3131-2006](https://doi.org/10.5194/acp-6-3131-2006), 2006. 13082

13, 13079–13117, 2013

Discussion Paper | Discussion Paper

Observations of biomass burning aerosol

T. Hamburger et al.

Title Page

Abstract

Introduction

Conclusions

References

Tables

Figures



Back

Close

Full Screen / Esc

Printer-friendly Version

Interactive Discussion



- Andreae, M. O., Artaxo, P., Fischer, H., Freitas, S. R., Grégoire, J.-M., Hansel, A., Hoor, P., Kormann, R., Krejci, R., Lange, L., Lelieveld, J., Lindner, W., Longo, K., Peters, W., de Reus, M., Scheeren, B., Silva Dias, M. A. F., Ström, J. M., J., van Velthoven, P. F. J., and Williams, J.: Transport of biomass burning smoke to the upper troposphere by deep convection in the equatorial region, *Geophys. Res. Lett.*, 28, 951–954, 2001. 13083
- 5 Andreae, M. O., Jones, C. D., and Cox, P. M.: Strong present-day aerosol cooling implies a hot future, *Nature*, 435, 1187–1190, 2005. 13082
- Ansmann, A., Baars, H., Tesche, M., Müller, D., Althausen, D., Engelmann, R., Pauliquevis, T., and Artaxo, P.: Dust and smoke transport from Africa to South America: lidar profiling over Cape Verde and the Amazon rainforest, *Geophys. Res. Lett.*, 36, L11802, doi:10.1029/2009GL037923, 2009. 13094
- 10 Bellouin, N., Boucher, O., Haywood, J., and Reddy, M. S.: Global estimate of aerosol direct radiative forcing from satellite measurements, *Nature*, 438, 1138–1141, 2005. 13083, 13101
- Boers, R., de Laat, A. T., Stein Zweers, D. C., and Dirksen, R. J.: Lifting potential of solar-heated aerosol layers, *Geophys. Res. Lett.*, 37, L24802, doi:10.1029/2010GL045171, 2010. 13096
- 15 Bond, T. C. and Bergstrom, R. W.: Light absorption by carbonaceous particles: an investigative review, *Aerosol Sci. Tech.*, 40, 27–67, doi:10.1080/02786820500421521, 2006. 13087
- Bond, T. C., Anderson, T. L., and Campbell, D.: Calibration and intercomparison of filter-based measurements of visible light absorption by aerosols, *Aerosol Sci. Tech.*, 30, 582–600, doi:10.1080/027868299304435, 1999. 13086
- 20 Bond, T. C., Streets, D. G., Yarber, K. F., Nelson, S. M., Woo, J.-H., and Klimont, Z.: A technology-based global inventory of black and organic carbon emissions from combustion, *J. Geophys. Res.*, 109, D14203, doi:10.1029/2003JD003697, 2004. 13083
- Bond, T. C., Doherty, S. J., Fahey, D. W., Forster, P. M., Berntsen, T., DeAngelo, B. J., Flanner, M. G., Ghan, S., Kärcher, B., Koch, D., Kinne, S., Kondo, Y., Quinn, P. K., Sarofim, M. C., Schultz, M. G., Schulz, M., Venkataraman, C., Zhang, H., Zhang, S., Bellouin, N., Guttiakunda, S. K., Hopke, P. K., Jacobson, M. Z., Kaiser, J. W., Klimont, Z., Lohmann, U., Schwarz, J. P., Shindell, D., Storelvmo, T., Warren, S. G., and Zender, C. S.: Bounding the role of black carbon in the climate system: a scientific assessment, *J. Geophys. Res. Atmos.*, doi:10.1002/jgrd.50171, 2013. 13089
- 25 Calderón, S., Iglesias, M., Ramoni, E., Hoffmann, P., Carrillo, J., Krejci, R., Hochschild, G., Gross, J., and Jochen, G.: Variación de la concentración de ozono troposférico en la estación

Observations of biomass burning aerosol

T. Hamburger et al.

[Title Page](#)

[Abstract](#)

[Introduction](#)

[Conclusions](#)

[References](#)

[Tables](#)

[Figures](#)

◀

▶

[Back](#)

[Close](#)

[Full Screen / Esc](#)

[Printer-friendly Version](#)

[Interactive Discussion](#)



- de investigación atmosférica “Alejandro de Humboldt” en Mérida, Venezuela, Ciencia e Ingeniería, 29, 97–106, 2008. 13084, 13086
- Chameides, W. L. and Bergin, M.: Soot takes center stage, *Science*, 297, 2214–2215, doi:10.1126/science.1076866, 2002. 13082
- 5 Draxler, R.: HYSPLIT4 user's guide, ERL ARL-230, Silver Spring, MD, 1999. 13088
- Edwards, D. P., Emmons, L. K., Gillett, J. C., Chu, A., Attié, J.-L., Giglio, L., Wood, S. W., Haywood, J., Deeter, M. N., Massie, S. T., Ziskin, D. C., and Drummond, J. R.: Satellite-observed pollution from Southern Hemisphere biomass burning, *J. Geophys. Res.*, 111, D14312, doi:10.1029/2005JD006655, 2006. 13083, 13094, 13100
- 10 Giannini, A., Kushnir, Y., and Cane, M. A.: Interannual variability of Caribbean rainfall, ENSO, and the Atlantic Ocean, *J. Climate*, 13, 297–311, doi:10.1175/1520-0442(2000)013<0297:IVOCRE>2.0.CO;2, 2000. 13099
- Giglio, L.: MODIS Collection 5 Active Fire Product User's Guide Version 2.4, Science Systems and Applications, Inc., Department of Geographical Sciences, University of Maryland, College Park, MD 20742, USA, 2010. 13089
- 15 Giglio, L., Descloitres, J., Justice, C. O., and Kaufman, Y. J.: An enhanced contextual fire detection algorithm for MODIS, *Remote Sens. Environ.*, 87, 273–282, doi:10.1016/S0034-4257(03)00184-6, 2003. 13089
- Giglio, L., van der Werf, G. R., Randerson, J. T., Collatz, G. J., and Kasibhatla, P.: Global estimation of burned area using MODIS active fire observations, *Atmos. Chem. Phys.*, 6, 957–974, doi:10.5194/acp-6-957-2006, 2006. 13089
- Grimm, A. M. and Tedeschi, R. G.: ENSO and extreme rainfall events in South America, *J. Climate*, 22, 1589–1609, doi:10.1175/2008JCLI2429.1, 2009. 13099
- Hao, W. M. and Liu, M.-H.: Spatial and temporal distribution of tropical biomass burning, *Global Biogeochem. Cy.*, 8, 495–503, doi:10.1029/94GB02086, 1994. 13083
- 25 Haywood, J. and Boucher, O.: Estimates of the direct and indirect radiative forcing due to tropospheric aerosols: a review, *Rev. Geophys.*, 38, 513–543, 2000. 13082
- Hoffmann, G.: Taking the pulse of the Tropical Water Cycle, *Science*, 301, 776–777, doi:10.1126/science.1085066, 2003. 13099
- 30 Janhäll, S., Andreae, M. O., and Pöschl, U.: Biomass burning aerosol emissions from vegetation fires: particle number and mass emission factors and size distributions, *Atmos. Chem. Phys.*, 10, 1427–1439, doi:10.5194/acp-10-1427-2010, 2010. 13085

Observations of biomass burning aerosol

T. Hamburger et al.

[Title Page](#)

[Abstract](#)

[Introduction](#)

[Conclusions](#)

[References](#)

[Tables](#)

[Figures](#)



[Back](#)

[Close](#)

[Full Screen / Esc](#)

[Printer-friendly Version](#)

[Interactive Discussion](#)



- Koch, D., Bond, T. C., Streets, D., Unger, N., and van der Werf, G. R.: Global impacts of aerosols from particular source regions and sectors, *J. Geophys. Res.*, 112, D02205, doi:10.1029/2005JD007024, 2007. 13083
- Koren, I., Remer, L. A., and Longo, K.: Reversal of trend of biomass burning in the Amazon, 5 *Geophys. Res. Lett.*, 34, L20404, doi:10.1029/2007GL031530, 2007. 13098
- Ley de Bosques y Gestión Forestal: Artículos 3,6,20,48–50 Gaceta Oficial N 38.946, Gaceta oficial, Gaceta Oficial de la República Bolivariana de Venezuela, 2008. 13098
- Lohmann, U. and Feichter, J.: Global indirect aerosol effects: a review, *Atmos. Chem. Phys.*, 5, 715–737, doi:10.5194/acp-5-715-2005, 2005. 13082
- 10 McPhaden, M. J., Zebiak, S. E., and Glantz, M. H.: ENSO as an integrating concept in Earth Science, *Science*, 314, 1740–1745, doi:10.1126/science.1132588, 2006. 13099
- Menon, S., Hansen, J., Nazarenko, L., and Luo, Y.: Climate effects of black carbon aerosols in China and India, *Science*, 297, 2250–2253, doi:10.1126/science.1075159, 2002. 13082
- Mertes, S., Dippel, B., and Schwarzenböck, A.: Quantification of graphitic carbon 15 in atmospheric aerosol particles by Raman spectroscopy and first application for the determination of mass absorption efficiencies, *J. Aerosol Sci.*, 35, 347–361, doi:10.1016/j.jaerosci.2003.10.002, 2004. 13087
- Mielonen, T., Arola, A., Komppula, M., Kukkonen, J., Koskinen, J., de Leeuw, G., and Lehtinen, K. E. J.: Comparison of CALIOP level 2 aerosol subtypes to aerosol types derived from 20 AERONET inversion data, *Geophys. Res. Lett.*, 36, L18804, doi:10.1029/2009GL039609, 2009. 13090
- Morales, J., Hermoso, M., Serrano, J., and Sanhueza, E.: Trace elements in the Venezuelan savannah atmosphere during dry and wet periods, with and without vegetation burning, *Atmos. Environ. A-Gen.*, 24, 407–414, doi:10.1016/0960-1686(90)90121-3, 1990. 13083, 13084, 25 13090
- Myhre, G.: Consistency between satellite-derived and modeled estimates of the direct aerosol effect, *Science*, 325, 187–190, doi:10.1126/science.1174461, 2009. 13082
- Naoe, H., Hasegawa, S., Heintzenberg, J., Okada, K., Uchiyama, A., Zaizen, Y., Kobayashi, E., and Yamazaki, A.: State of mixture of atmospheric submicrometer black carbon particles and its effect on particulate light absorption, *Atmos. Environ.*, 43, 1296–1301, 30 doi:10.1016/j.atmosenv.2008.11.031, 2009. 13087

**Observations of
biomass burning
aerosol**

T. Hamburger et al.

[Title Page](#)[Abstract](#)[Introduction](#)[Conclusions](#)[References](#)[Tables](#)[Figures](#)[◀](#)[▶](#)[◀](#)[▶](#)[Back](#)[Close](#)[Full Screen / Esc](#)[Printer-friendly Version](#)[Interactive Discussion](#)

Observations of biomass burning aerosol

T. Hamburger et al.

[Title Page](#)

[Abstract](#)

[Introduction](#)

[Conclusions](#)

[References](#)

[Tables](#)

[Figures](#)

◀

▶

◀

▶

[Back](#)

[Close](#)

[Full Screen / Esc](#)

[Printer-friendly Version](#)

[Interactive Discussion](#)



- Novakov, T., Ramanathan, V., Hansen, J. E., Kirchstetter, T. W., Sato, M., Sinton, J. E., and Sathaye, J. A.: Large historical changes of fossil-fuel black carbon aerosols, *Geophys. Res. Lett.*, 30, 1324, doi:10.1029/2002GL016345, 2003. 13082
- Omar, A. H., Winker, D. M., Vaughan, M. A., Hu, Y., Trepte, C. R., Ferrare, R. A., Lee, K.-P., Hostetler, C. A., Kittaka, C., Rogers, R. R., Kuehn, R. E., and Liu, Z.: The CALIPSO Automated Aerosol Classification and Lidar Ratio Selection Algorithm, *J. Atmos. Oceanic Technol.*, 26, 1994–2014, doi:10.1175/2009JTECHA1231.1, 2009. 13090
- Ramanathan, V. and Carmichael, G.: Global and regional climate changes due to black carbon, *Nature Geosci.*, 1, 221–227, 2008. 13082
- Ramanathan, V., Ramana, M. V., Roberts, G., Kim, D., Corrigan, C., Chung, C., and Winker, D.: Warming trends in Asia amplified by brown cloud solar absorption, *Nature*, 448, 575–578, 2007. 13083
- Rissler, J., Vestin, A., Swietlicki, E., Fisch, G., Zhou, J., Artaxo, P., and Andreae, M. O.: Size distribution and hygroscopic properties of aerosol particles from dry-season biomass burning in Amazonia, *Atmos. Chem. Phys.*, 6, 471–491, doi:10.5194/acp-6-471-2006, 2006. 13083, 13094
- Rizzo, L. V., Artaxo, P., Müller, T., Wiedensohler, A., Paixão, M., Cirino, G. G., Arana, A., Swietlicki, E., Roldin, P., Fors, E. O., Wiedemann, K. T., Leal, L. S. M., and Kulmala, M.: Long term measurements of aerosol optical properties at a primary forest site in Amazonia, *Atmos. Chem. Phys.*, 13, 2391–2413, doi:10.5194/acp-13-2391-2013, 2013. 13091, 13094
- Rondón, A. and Sanhueza, E.: Seasonal variation of gaseous HNO_3 and NH_3 at a Tropical Savannah site, *J. Atmos. Chem.*, 11, 245–254, doi:10.1007/BF00118351, 1990. 13084
- Roy, D., Jin, Y., Lewis, P., and Justice, C.: Prototyping a global algorithm for systematic fire-affected area mapping using {MODIS} time series data, *Remote Sens. Environ.*, 97, 137–162, doi:10.1016/j.rse.2005.04.007, 2005. 13089
- Roy, D., Boschetti, L., Justice, C., and Ju, J.: The collection 5 MODIS burned area product – global evaluation by comparison with the MODIS active fire product, *Remote Sens. Environ.*, 112, 3690–3707, doi:10.1016/j.rse.2008.05.013, 2008. 13089
- Sakaeda, N., Wood, R., and Rasch, P. J.: Direct and semidirect aerosol effects of southern African biomass burning aerosol, *J. Geophys. Res.*, 116, D12205, doi:10.1029/2010JD015540, 2011. 13096

**Observations of
biomass burning
aerosol**

T. Hamburger et al.

[Title Page](#)[Abstract](#)[Introduction](#)[Conclusions](#)[References](#)[Tables](#)[Figures](#)[|◀](#)[▶|](#)[◀](#)[▶|](#)[Back](#)[Close](#)[Full Screen / Esc](#)[Printer-friendly Version](#)[Interactive Discussion](#)

Sanhueza, E., Rondón, A., and Romero, J.: Airborne particles in the Venezuelan savannah during burning and non-burning periods, *Atmos. Environ.*, 21, 2227–2231, doi:10.1016/0004-6981(87)90354-4, 1987. 13083, 13085, 13094

5 Sanhueza, E., Crutzen, P. J., and Fernández, E.: Production of boundary layer ozone from tropical American Savannah biomass burning emissions, *Atmos. Environ.*, 33, 4969–4975, doi:10.1016/S1352-2310(99)00301-5, 1999. 13083

Schmeissner, T., Krejci, R., Ström, J., Birmili, W., Wiedensohler, A., Hochschild, G., Gross, J., Hoffmann, P., and Calderon, S.: Analysis of number size distributions of tropical free tropospheric aerosol particles observed at Pico Espejo (4765 m a.s.l.), Venezuela, *Atmos. Chem. Phys.*, 11, 3319–3332, doi:10.5194/acp-11-3319-2011, 2011. 13084, 13085, 13086

Schwarz, J. P., Gao, R. S., Spackman, J. R., Watts, L. A., Thomson, D. S., Fahey, D. W., Ryerson, T. B., Peischl, J., Holloway, J. S., Trainer, M., Frost, G. J., Baynard, T., Lack, D. A., de Gouw, J. A., Warneke, C., and Del Negro, L. A.: Measurement of the mixing state, mass, and optical size of individual black carbon particles in urban and biomass burning emissions, *Geophys. Res. Lett.*, 35, L13810, doi:10.1029/2008GL033968, 2008. 13087

15 Shindell, D., Kuylenstierna, J. C. I., Vignati, E., van Dingenen, R., Amann, M., Klimont, Z., Anenberg, S. C., Muller, N., Janssens-Maenhout, G., Raes, F., Schwartz, J., Faluvegi, G., Pozzoli, L., Kupiainen, K., Höglund-Isaksson, L., Emberson, L., Streets, D., Ramanathan, V., Hicks, K., Oanh, N. T. K., Milly, G., Williams, M., Demkine, V., and Fowler, D.: Simultaneously mitigating near-term climate change and improving human health and food security, *Science*, 335, 183–189, doi:10.1126/science.1210026, 2012. 13083

20 Stohl, A., Forster, C., Frank, A., Seibert, P., and Wotawa, G.: Technical note: The Lagrangian particle dispersion model FLEXPART version 6.2, *Atmos. Chem. Phys.*, 5, 2461–2474, doi:10.5194/acp-5-2461-2005, 2005. 13095

25 Streets, D. G., Bond, T. C., Lee, T., and Jang, C.: On the future of carbonaceous aerosol emissions, *J. Geophys. Res.*, 109, D24212, doi:10.1029/2004JD004902, 2004. 13083, 13098, 13100

30 Ten Hoeve, J. E., Jacobson, M. Z., and Remer, L. A.: Comparing results from a physical model with satellite and in situ observations to determine whether biomass burning aerosols over the Amazon brighten or burn off clouds, *J. Geophys. Res.*, 117, D08203, doi:10.1029/2011JD016856, 2012. 13096

**Observations of
biomass burning
aerosol**

T. Hamburger et al.

Torres, O., Chen, Z., Jethva, H., Ahn, C., Freitas, S. R., and Bhartia, P. K.: OMI and MODIS observations of the anomalous 2008–2009 Southern Hemisphere biomass burning seasons, *Atmos. Chem. Phys.*, 10, 3505–3513, doi:10.5194/acp-10-3505-2010, 2010. 13098

van der Werf, G. R., Randerson, J. T., Collatz, G. J., Giglio, L., Kasibhatla, P. S., Arellano, A. F.,
5 Olsen, S. C., and Kasischke, E. S.: Continental-scale partitioning of fire emissions during the 1997 to 2001 El Niño/La Niña period, *Science*, 303, 73–76, doi:10.1126/science.1090753, 2004. 13099

van Poppel, L. H., Friedrich, H., Spinsby, J., Chung, S. H., Seinfeld, J. H., and Buseck, P. R.:
10 Electron tomography of nanoparticle clusters: implications for atmospheric lifetimes and radiative forcing of soot, *Geophys. Res. Lett.*, 32, L24811, doi:10.1029/2005GL024461, 2005. 13083

Virkkula, A.: Correction of the Calibration of the 3-wavelength Particle Soot Absorption Photometer (3 PSAP), *Aerosol Sci. Tech.*, 44, 706–712, doi:10.1080/02786826.2010.482110, 2010. 13086

15 Virkkula, A., Ahlquist, N. C., Covert, D. S., Arnott, W. P., Sheridan, P. J., Quinn, P. K., and Coffman, D. J.: Modification, calibration and a field test of an instrument for measuring light absorption by particles, *Aerosol Sci. Tech.*, 39, 68–83, doi:10.1080/027868290901963, 2005. 13086

20 Winker, D. M., Vaughan, M. A., Omar, A., Hu, Y., Powell, K. A., Liu, Z., Hunt, W. H., and Young, S. A.: Overview of the CALIPSO Mission and CALIOP Data Processing Algorithms, *J. Atmos. Oceanic Technol.*, 26, 2310–2323, doi:10.1175/2009JTECHA1281.1, 2009. 13089

25 Yang, M., Howell, S. G., Zhuang, J., and Huebert, B. J.: Attribution of aerosol light absorption to black carbon, brown carbon, and dust in China – interpretations of atmospheric measurements during EAST-AIRE, *Atmos. Chem. Phys.*, 9, 2035–2050, doi:10.5194/acp-9-2035-2009, 2009. 13087

[Title Page](#)[Abstract](#)[Introduction](#)[Conclusions](#)[References](#)[Tables](#)[Figures](#)[|◀](#)[▶|](#)[◀](#)[▶](#)[Back](#)[Close](#)[Full Screen / Esc](#)[Printer-friendly Version](#)[Interactive Discussion](#)

Table 1. Arithmetic mean and standard deviation of observed parameters at Pico Espejo for different seasons and air masses; relative humidity RH (%), temperature t ($^{\circ}\text{C}$), number of fire events since the last precipitation event according to the trajectory analysis (#), ambient aerosol volume concentration V ($\mu\text{m}^3 \text{cm}^{-3}$), ambient aerosol number concentration N (cm^{-3}), heated aerosol number concentration $N_{300\text{ }^{\circ}\text{C}}$ (cm^{-3}), ratio of heated and ambient aerosol number concentration $N_{300\text{ }^{\circ}\text{C}}/N$ (0–1), and absorption coefficient b_{abs} (M m^{-1}). To convert the ambient concentrations and b_{abs} to standard temperature and pressure please use $\text{stp} = 1.77 \pm (0.01)\text{amb.}$

Season	RH (%)	t (°C)	Fire events (#)	V ($\mu\text{m}^3 \text{cm}^{-3}$)	N (cm^{-3})	$N_{300^\circ\text{C}}$ (cm^{-3})	$N_{300^\circ\text{C}}/N$ (0–1)	b_{abs} (M m^{-1})
Boundary layer								
dry	82 ± 8.7	1.8 ± 1.9	4.8 ± 11	1.4 ± 1.3	730 ± 470	510 ± 420	0.64 ± 0.19	0.91 ± 1.2
	86 ± 7.9	1.7 ± 2.1	0.6 ± 2.4	0.49 ± 0.41	480 ± 260	230 ± 130	0.46 ± 0.14	0.32 ± 0.38
Lower free troposphere								
dry	45 ± 27	0.76 ± 2.2	0.1 ± 0.9	0.47 ± 0.70	480 ± 310	260 ± 290	0.50 ± 0.20	0.36 ± 0.59
	67 ± 25	-0.02 ± 1.9	0.0 ± 0.3	0.19 ± 0.25	390 ± 270	150 ± 94	0.39 ± 0.16	0.15 ± 0.26



**Observations of
biomass burning
aerosol**

T. Hamburger et al.

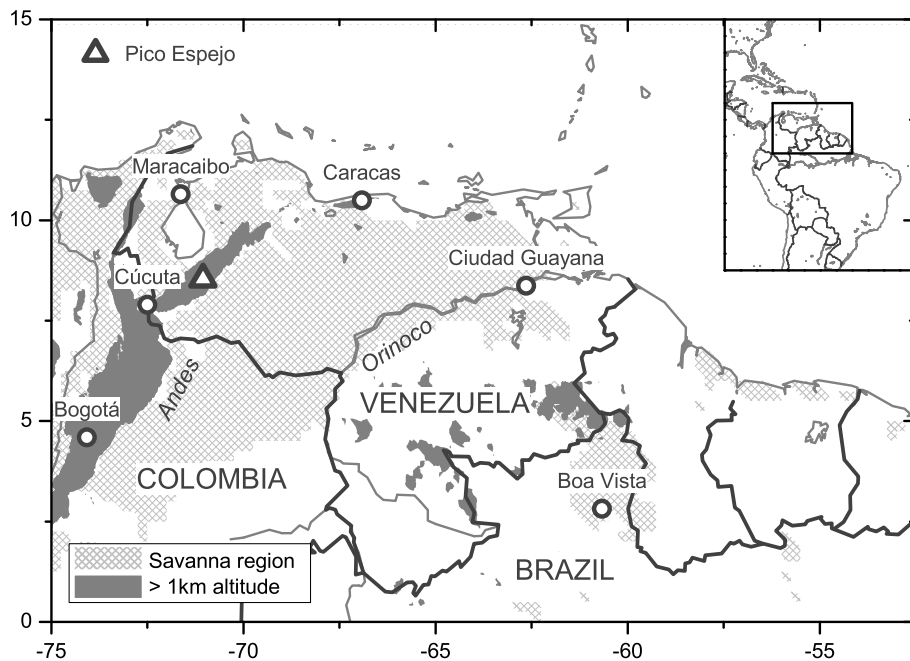


Fig. 1. Map of the northern part of South America. The triangle indicates the position of the Pico Espejo Atmospheric Research Station Alexander von Humboldt (4765 m a.s.l.) in Venezuela.

[Title Page](#)[Abstract](#)[Introduction](#)[Conclusions](#)[References](#)[Tables](#)[Figures](#)[|◀](#)[▶|](#)[◀](#)[▶](#)[Back](#)[Close](#)[Full Screen / Esc](#)[Printer-friendly Version](#)[Interactive Discussion](#)

Observations of biomass burning aerosol

T. Hamburger et al.

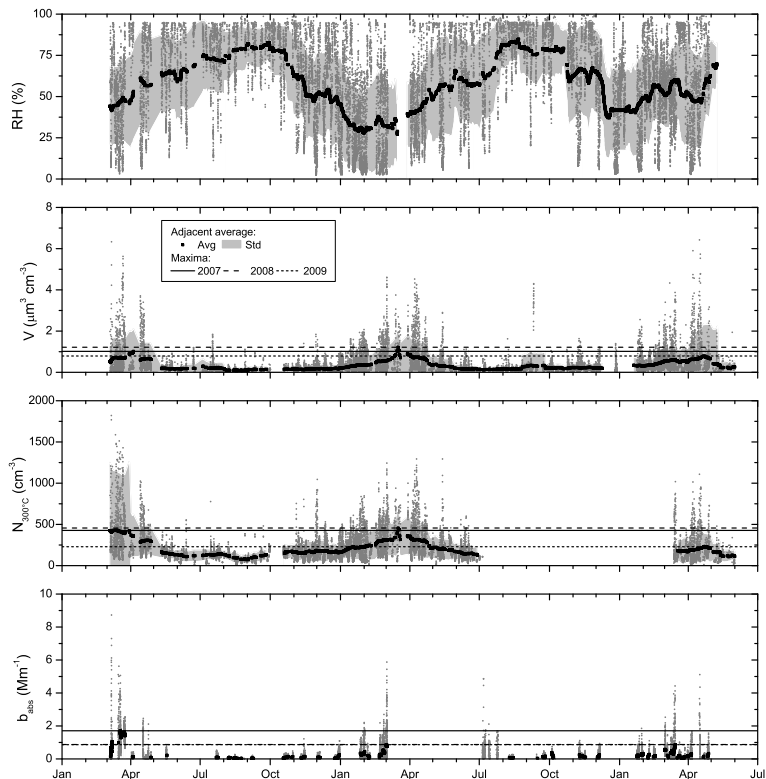


Fig. 2. Time series of data observed in the LFT comprising relative humidity RH (%), ambient aerosol volume concentration V ($\mu\text{m}^3 \text{cm}^{-3}$), heated aerosol number concentration $N_{300^\circ\text{C}}$ (cm^{-3}), and absorption coefficient b_{abs} (Mm^{-1}). The small dots in dark grey indicate 15 min averages, the black squares the one monthly adjacent average and its standard deviation in light grey. Horizontal lines show the maxima of the one monthly adjacent average for each dry season.

[Title Page](#)

[Abstract](#)

[Introduction](#)

[Conclusions](#)

[References](#)

[Tables](#)

[Figures](#)

[|◀](#)

[▶|](#)

[◀](#)

[▶](#)

[Back](#)

[Close](#)

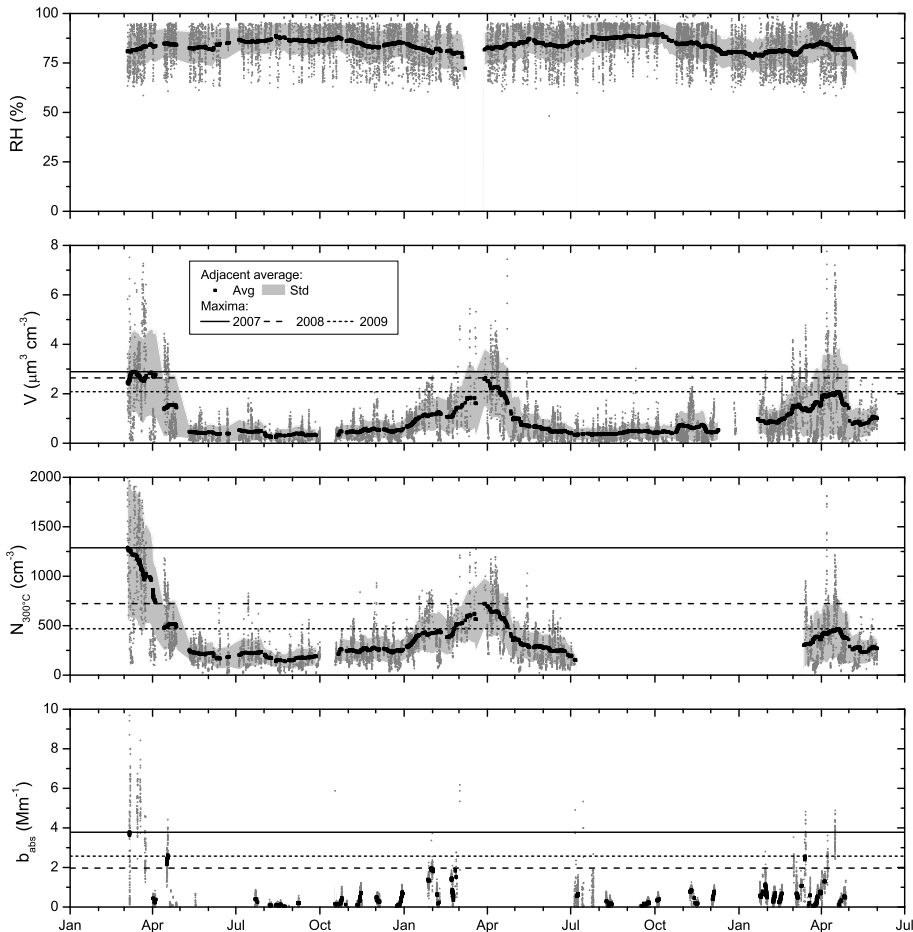
[Full Screen / Esc](#)

[Printer-friendly Version](#)

[Interactive Discussion](#)

**Observations of
biomass burning
aerosol**

T. Hamburger et al.

**Fig. 3.** Same as Fig. 2 but for data observed in the BL.[Printer-friendly Version](#)[Interactive Discussion](#)[Title Page](#)[Abstract](#)[Introduction](#)[Conclusions](#)[References](#)[Tables](#)[Figures](#)[Close](#)[Full Screen / Esc](#)

Observations of biomass burning aerosol

T. Hamburger et al.

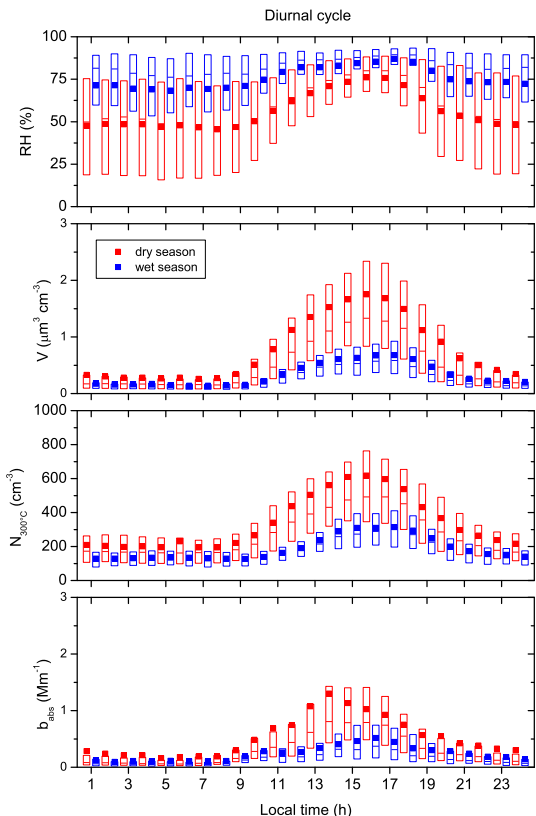
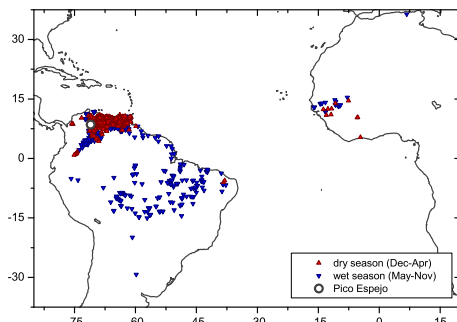


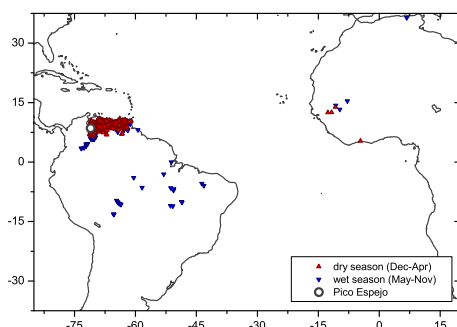
Fig. 4. Diurnal cycles of relative humidity RH (%), ambient aerosol volume concentration V ($\mu\text{m}^3 \text{cm}^{-3}$), heated aerosol number concentration $N_{300^\circ\text{C}}$ (cm^{-3}), and absorption coefficient b_{abs} (Mm^{-1}). The bars indicate 25th percentile–median–75th percentile, the squares the arithmetic mean. Red colour indicates observations during the dry season, blue colour during the wet season. The time is local time (UTC-4.5 h).

Observations of biomass burning aerosol

T. Hamburger et al.



(a)



(b)

Fig. 5. Possible fire events affecting the observations according to the trajectory analysis (~ 10 days). Red triangles represent the Venezuelan dry season, blue triangles its wet season. **(a)** shows all possible fire events not accounting for precipitation along the air mass transport path way. **(b)** shows all fire events excluding events with precipitation along the transport path way.

Title Page

Abstract

Introduction

Conclusions

References

Tables

Figures



Back

Close

Full Screen / Esc

[Printer-friendly Version](#)

Interactive Discussion



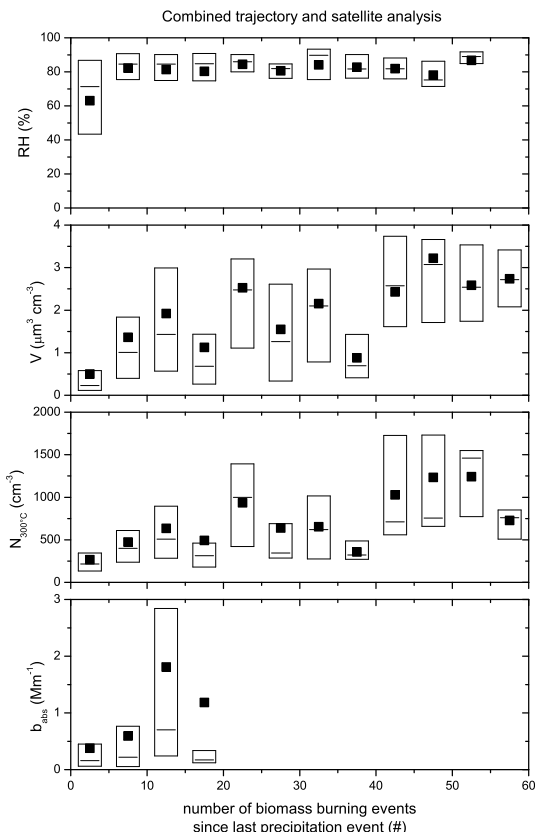


Fig. 6. Relative humidity RH (%), ambient aerosol volume concentration V ($\mu\text{m}^3\text{cm}^{-3}$), heated aerosol number concentration $N_{300^\circ\text{C}}$ (cm^{-3}), and absorption coefficient b_{abs} (Mm^{-1}) versus the number of fire events detected since the last precipitation event according to the trajectory analysis (-10 days).

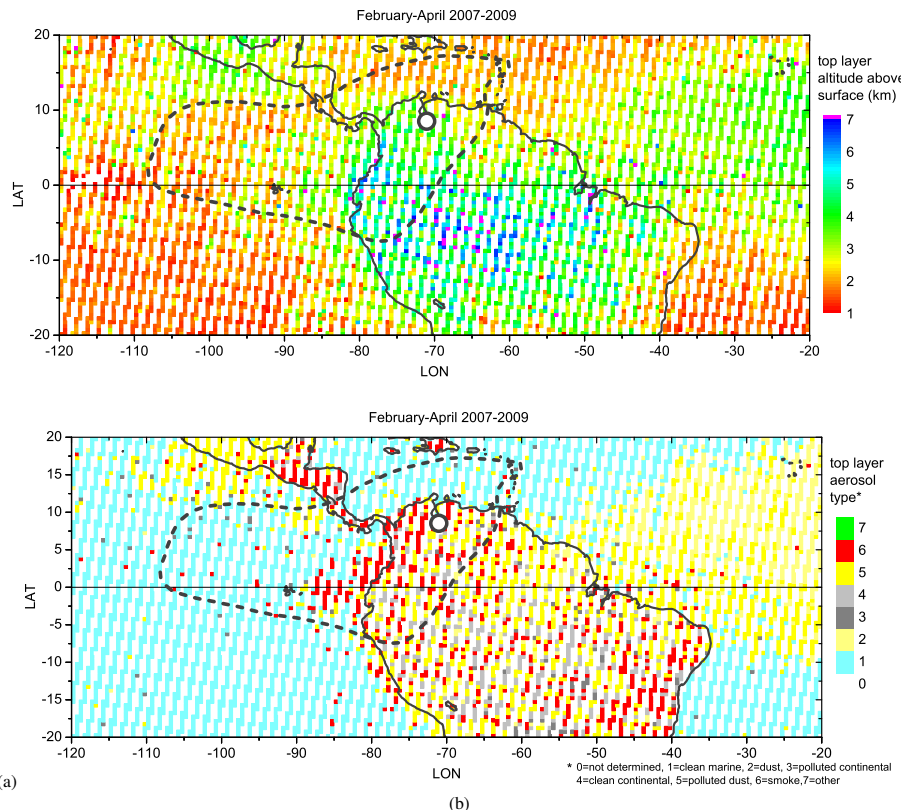


Fig. 7. CALIPSO satellite observations averaged for February–April for the years 2007–2009. **(a)** shows the altitude above the surface of the upper most aerosol layer and **(b)** its dominating aerosol type (see Sect. 2.4 for details). Both parameters are retrieved from the LIDAR Level 2 5 km Aerosol Layer product. The dashed line indicates the average area which is covered by 10 day forward trajectories within the same period.

Discussion paper | Discussion paper | Discussion paper | Discussion paper

Discussion Page

Discussion Paper |

Title Page	
Abstract	Introduction
Conclusions	References
Tables	Figures
◀	▶
◀	▶
Back	Close
Full Screen / Esc	
Printer-friendly Version	
Interactive Discussion	



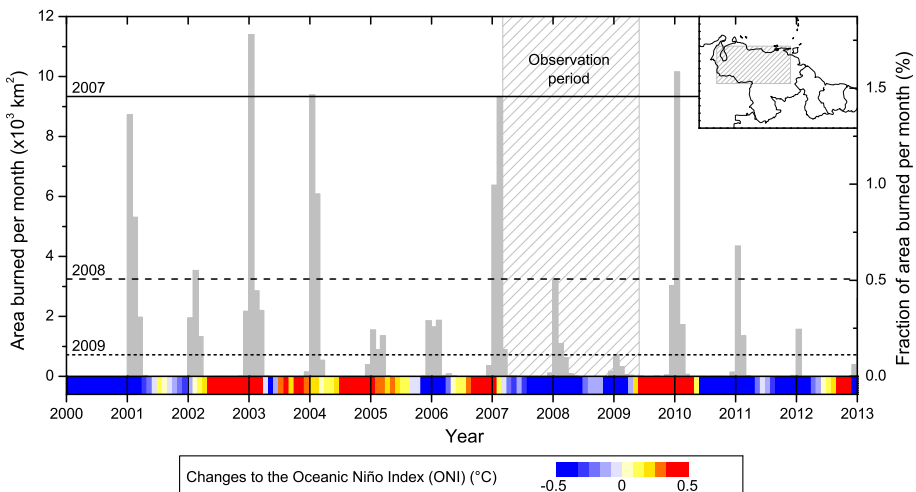


Fig. 8. Time series of the area affected by fires for the wider region of Venezuela (km^2) (see Sect. 2.4 for details). The data is based on MODIS satellite observations. The horizontal lines indicate the maxima for the dry season during the observation period at the Pico Espejo. The colour coded x-axes shows periods with El Niño conditions (red) and La Niña conditions (blue).